JURNAL APTEK

Artikel Ilmiah Aplikasi Teknologi
homepage: http://journal.upp.ac.id/index.php/aptek

Vol. 16. No. 2
p-ISSN 2085-2630
e-ISSN 2655-9897

Effect of Recondition of Fracture Shaft Palm Lorry Using The Shielded Metal Arc Welding Process

Lukman Hakim Nasution[*1, 2, 3], Eka Ariefyanto Putra[1], Gapar[1], Fajar Budiman[1], Rama Yoedha Satria[1], Andersen[1], Sofyan Hadi[2], Ferry Adriyan[2], Nasrol Akmal[2], Rinaldi[3], Nazaruddin[3], Safril Safar[3], Heri Suripto[4]

[1)]Badan Perencanaan Pembangunan Daerah, Penelitian dan Pengembangan Provinsi Riau
Pekanbaru-Riau
lukman_n82@yahoo.com

[2)] Riau Science Techno Park Riau
Pekanbaru-Riau

[3)]Sekolah Tinggi Teknologi Pekanbaru
Pekanbaru-Riau

[4)]Universitas Pasir Pengaraian
Rokanhulu-Riau

A B S T R A C T

Examination and analysis of the 2,640 working hours AISI 1045 palm lorry shaft fracture were carried out to determine the effect of reconditioning using Shielded Metal Arc Welding on the reliability of the shaft. Laboratory test results and analysis showed that the shaft experienced a static brittle fracture at an angle between 65 mm diameter and 90 mm diameter. For a long time, evidence of weld defects in the form of inclusions, porosity, and cold cracks in the Heat Affective Zone has been observed. The various hardness levels in the weld metal are 200 to 210 HV; HAZ is 280 to 386 HV, and base metal is 202 to 210 HV due to oxygen affecting on shaft's mechanical qualities deterioration. When the martensitic structure is produced, the carbon equivalent value rises to 15.66%, over the minimum value of 0.65%, reducing shaft reliability and triggering the occurrence of static brittle fracture. The macro-micro structure at the initial area of crack and fracture is bainite and ferrite-pearlite, while the shaft base material is ferrite-pearlite. Furthermore, there is a difference in tensile strength between the shaft material and the power of the electrodes utilized in the reconditioning process. From this experiment, the recondition

Keywords: AISI 1045 shaft; SMAW; reconditioning; and static brittle fracture.

1. INTRODUCTION

Welding is an effective and versatile method for joining similar materials, including metals and their alloys. This method uses a combination of heat and pressure to form atomic-level bonds in the parent metals, resulting in the strength of the joint. Shielded Metal Arc Welding (SMAW), commonly utilized in industry, the sub-classification depends on the electrode to create an arc to the work metal that can be consumed or not [1]. Current and welding speed are the primary parameters, followed by preheat temperature [2]. The welding process is also a cost-effective and efficient permanent joining technique that uses E 7016 or E 7018 electrodes for AISI 1045 steel types, and the results of the welds may be tested using tensile and compression tests [3, 4]. The AISI 1045 steel is commonly used in industry; this type of steel is not corrosion-resistant but has outstanding strength, toughness, and wear resistance [5-6]. Based on microstructural studies, performing the SMAW process on AISI1045 steel is preferable by adding preheat and Post-Weld Heat Treatment (PWHT) [7]. The parameters of SMAW welding on AISI 1045 steel include welding current and welding speed, significantly affecting the ultimate tensile strength in the no-pre-heat and preheat conditions. In a case without preheating, there is an increase in hardness without decreasing strength [8].

The SMAW welding procedures use low and high arc energy levels, such as E 7016 or E 7018 electrodes with diameters of 3.2 mm and 5.0 mm [9], which can be applied for AISI 1045 steels. Likewise, changes in the arc contact's, hardness, and microstructure may emerge due to the welding process's current,

Corresponding Author:
✉ **Lukman Hakim Nasution**
Accepted on: 2024-06-28

DOI: 10.30606/aptek.v16i2.2694

voltage, and speed. The interface microstructure of the weld metal and base metal also displays the difference between the fusion and HAZ area. This interfacial fusion zone is characterized by fine ferrite grains as relatively strain-free grains due to differences in the degree of solidification of the weld metal and heat input [10]. The amount of heat energy per unit length of the weld is the heat input experienced by the metal during the welding process. The heat input occurring in the metal is influenced by heat conductivity, weld geometry, and thickness, as well as the type of joint and the shape of the welding groove, as well as the welding technique and parameters applied to the weld metal [11-13]. Heat input is useful for estimating the microstructure, its relation to the mechanical properties of welded joints, and the occurrence of weld defects such as cold cracks [14, 15]. Welding flux is another important factor that influences the features, solidification heat flow rate, and mechanical properties of the metal. Similarly, preheating, post-heating, polarity, and inter-pass temperature are the primary parameters that influence the mechanical properties of welded metal [16]. As the welding current increases, the metal's yield, tensile, and fracture strength will increase. Aside from metal strength, welding current influences the growth in inclusion and corrosion rates as heat input increases [17]. The residual stress can also be observed in the structure and microhardness, which lies between the weld metal and base metal boundaries due to the contraction-expansion effect caused by the phase transformation and the difference in cooling rates. This can result in welded metal failure in the form of residual stress area fractures and HAZ due to inclusions in different sections of the weld zone close to each other [18].

Preheat will lower the residual stresses that vary for each weld seam as well as the interface's mechanical mismatch [19]. Including Carbon Equivalent (CE) content> 0.35% by providing preheating, causing the overall heat input to increase. Steel with CE>0.35% has high hardenability because martensitic structures are easily formed. Combining chemical composition and cooling rate can form a phase sensitive to cracks' appearance. The carbon equivalent value and crack parameter are positively correlated; the sensitivity of steel to cold cracks will decrease if the carbon equivalent value and crack parameter also decrease [20]. While the analysis of the micro-macro structure is influenced by the type of electrode used, for example, the SMAW process using the E 7016 electrode will give a narrower HAZ, so the mechanical properties are higher compared to using the E 6013 and E 7018 electrodes [5, 21, 22]. Due to the fast-cooling rate, specimens without preheating will exhibit columnar ferrite in the weld metal microstructure. This condition can increase hardness in the HAZ, which is higher than the weld metal; nevertheless, the toughness of the weld metal is higher without pre or post-heat treatment [11]. The differences in the microstructure caused by thermal cycles in the HAZ, base metal, and fusion zone are related to mechanical qualities. Increasing the number of thermal cycles results in transforming the ferrite morphology in the HAZ [23, 24].

Hot or cold cracking can occur in the weld metal, regardless of the impact of the filler metal composition, and is associated with the growth of metal grains in the HAZ [25]. The degree of softening or hardening in the HAZ is directly related to the welding parameters. The HAZ width of the sample is directly related to the heat input used as a determinant of the failure location [26]. Based on the metallurgical analysis, it is characterized by the presence of weld metal failure due to phase change and creep embrittlement in the HAZ. Cracking and fracture due to embrittlement starts at the fusion line and propagates in the coarse-grained HAZ, which are interconnected with the creep cavities [27], and due to oxidation of the base metal and HAZ [28]. The hardness test at HAZ [29] also demonstrates that welding speed and cooling rate influence the volume proportion of martensite and metal hardness [30, 31].

2. MATERIAL AND METHODOLOGY

Investigation of reconditioning fractured shaft of oil palm lorry has been carried out. The information about reconditioning process compared with the AWS method is listed in Table 1. The macro-fractographic analysis, which was carried out using a CH 9435 stereomicroscope, of fractured shaft testing after 2,640 working hours began with a direct examination of the surface of the crack side is described in Figure 1-3. It is important to determine the shape or characteristics of the shaft's failure, including the initial search for cracks and fractures. Testing was carried out to assess the reconditioning effect of SMAW on the AISI 1045 shaft. The chemical composition testing was performed using the Metorex spectrometer; hardness testing was performed using Frank Finite's Hardness Vickers; metallography and SEM-EDX were used to calculate the carbon equivalent value.

Table1. Data on reconditioning.

Reconditioning of AISI 1045 carbon steel	
Completed Reconditioning	AWS-compliant reconditioning [20]
Preheat is not performed. Post Weld Heat is not performed. E 6013 type of electrode. AC type. Layer cleaning is imperfect. 2F Position. Post-welding water cooling.	Preheat between 200°C to 300°C. Post Weld Heat between 600°C to 650°C. Electrode type E 7016 or E 7018 DCRP current type Every single layer of cleaning must be flawless. 1G/5G Position Cooling uses a CCT diagram and is calculated by equation $\Delta t_{\frac{8}{5}} = \frac{q/v}{500-T_0} - \frac{1}{800-T_0}$, where ΔT8/5 is the time spent cooling between 800 °C and 500 °C, T_0 is the initial temperature (°C), q is heat input (kJ/mm), v is welding speed (mm/s), and k is thermal conductivity (J/mm. s-1K-1)].

Figure 1. The fracture shaft of oil palm lorry S45C 2,640 working hours.

Figure 2. The fracture shaft measurements, 2,640 working hours.

Figure 3. The fracture shaft is between Ø65 mm to Ø90 mm.

3. RESULTS AND DISCUSSIONS

According to the results of macrofractographic analysis based on images from Figures 9, 10, and 11, the shaft has a static brittle fracture, specifically at the

corner between 65 mm and 90 mm in diameter. Static brittle fracture has been occurring for a long time due to the vast number of inclusions, porosity, and cold fractures caused by varied hardness levels. The macro-microstructure of AISI1045 steel changes at the initial area of crack and fracture, where the usual macro-microstructure is ferrite-pearlite, becoming martensitic as a marker and trigger for static brittle fracture. Figure 12 shows micro-crack occurrence because of reconditioning in cold crack HAZ types. The martensite-austenite microstructure in Figure 13 is in the form of trans-granular cracks, and Figure 14 with arrows indicates that the macro photo of the metallographic sample of the longitudinal section of the fracture area shows reconditioning and the initial fracture starts from the weld material. Figures 15 and 16 indicate that the microstructure is martensite, with cracks in the HAZ and inclusions caused by the action of SMAW heat. The shape of the crack is a cold crack in the weld material. There is a defect in the shaft due to the reconditioning process. Figure 17 and Table 2 show a macro photo of the metallographic sample in the longitudinal section of the fracture area and the difference in hardness due to reconditioning using SMAW.

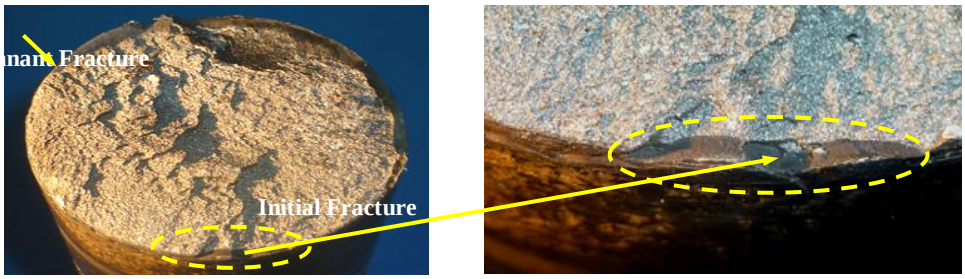

Figure 9. The lorry axle's initial fracture.

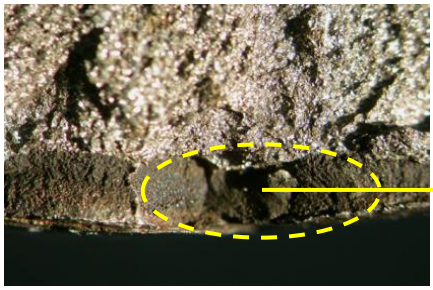

Figure 10. Photo macro at 12x magnification.

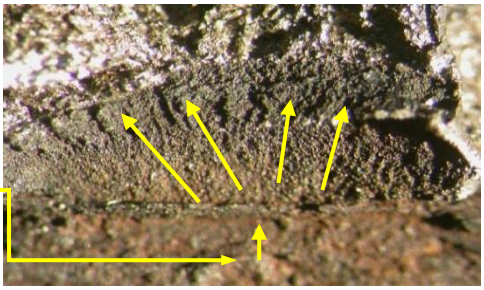

Figure 11. Photo macro at 25x magnification.

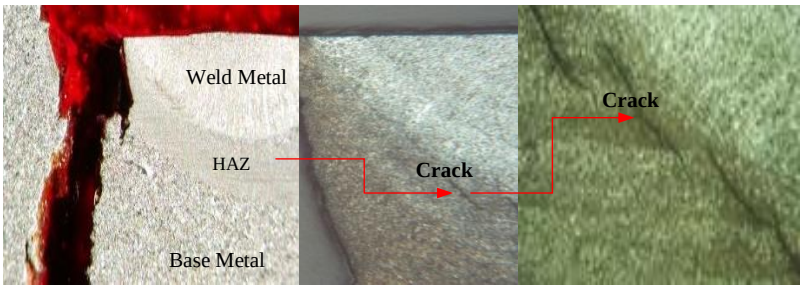

Figure 12. Photo HAZ micro crackat 25x magnification.

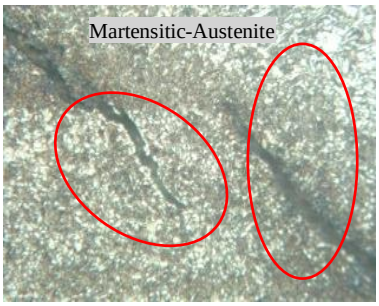

Figure 13. Micro structure of reconditioned oil palm lorry shaft at 500x magnification.

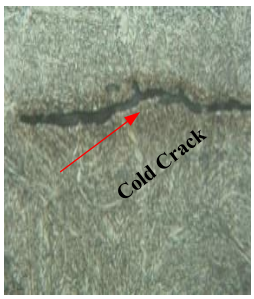

Figure 14. Micro structure of martensitic-austenite in HAZ at 200x magnification

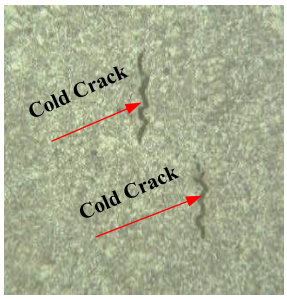

Figure 15. Crack shape in HAZat 500x

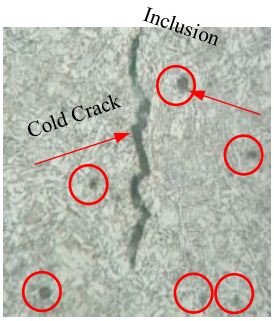

Figure 16. Cold crack and inclusion on reconditioned shaft at 500x magnification

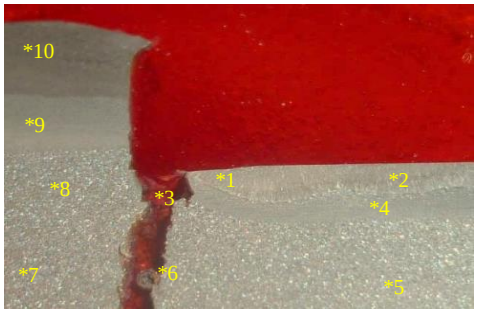

Figure 17. Macro photo of the hardness test sample

Table 2. The differences in shaft hardness caused by SMAW reconditioning.

No	Hardness Value (HV)	Area
1	204	Weld Metal
2	210	Weld Metal
3	381	HAZ
4	386	HAZ
5	206	Base Metal
6	202	Base Metal
7	210	Base Metal
8	202	Base Metal
9	280	HAZ
10	200	Weld Metal

According to the hardness test results, there is a variation in the hardness level between the weld metal, HAZ, and base metal after the reconditioning process. The rise in stress in the HAZ due to reconditioning corresponds to the increase in hardness level. Stress and hardness levels did not increase and even decreased in areas that did not receive reconditioning. While the chemical composition after reconditioning is also analyzed to determine the level and influence of carbon equivalent due to the SMAW process. According to the

results of the SEM-EDX test, the square area in Figure 18 has a carbon equivalent value of 28.83%, a ferrous content of 38.28%, and a presence of oxygen element of 31.69%, which causes cracks and weld porosity. It is 0.65% higher than the standard AISI 1045 carbon equivalent shaft, having a ferrous content of 98.981%.

The square area in Figure 19 has a carbon equivalent of 10.34%, a ferrous content of 78.50%, and a presence of oxygen of 10.32%, which causes cracks and weld porosity. Compared to the standard AISI 1045 carbon equivalent shaft, it is 0.65% with a ferrous content of 98.981%. Whereas at site three in Figure 20, the carbon equivalent is 13.41%, the ferrous content is 18.36%, and the presence of oxygen is 16.33%, which causes cracks and weld porosity. Compared to the standard AISI 1045 carbon equivalent shaft, it is 0.65% with a ferrous content of 98.981%.

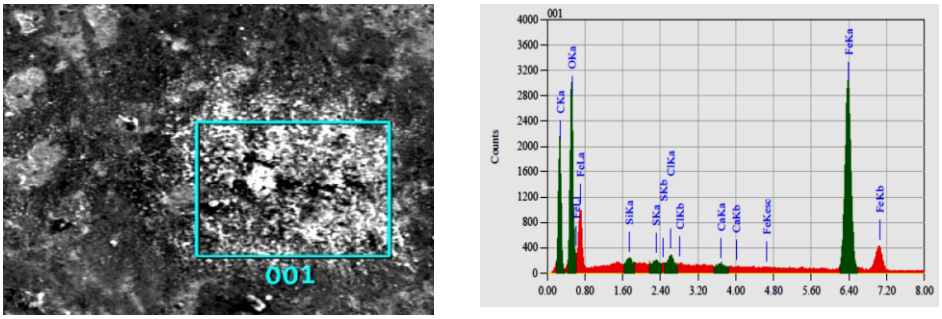

Figure 18. Photographs and graphs of fracture surfaces at location one

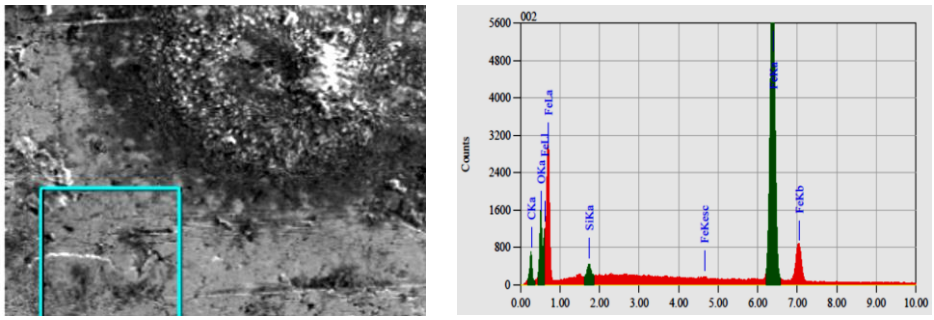

Figure 19. Photographs and graphs of fracture surfaces at location two.

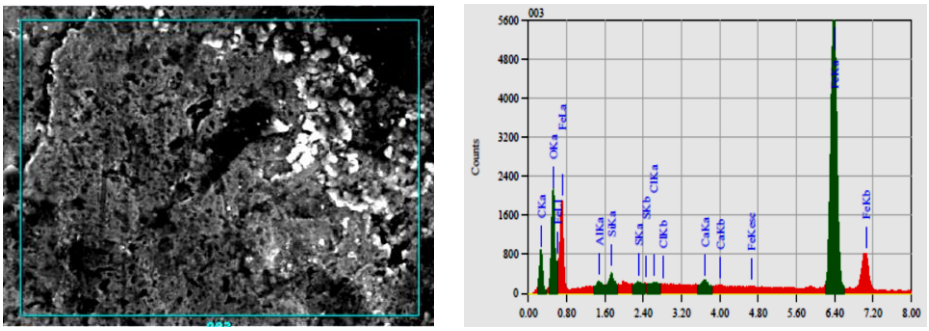

Figure 20. Photographs and graphs of fracture surfaces at location three

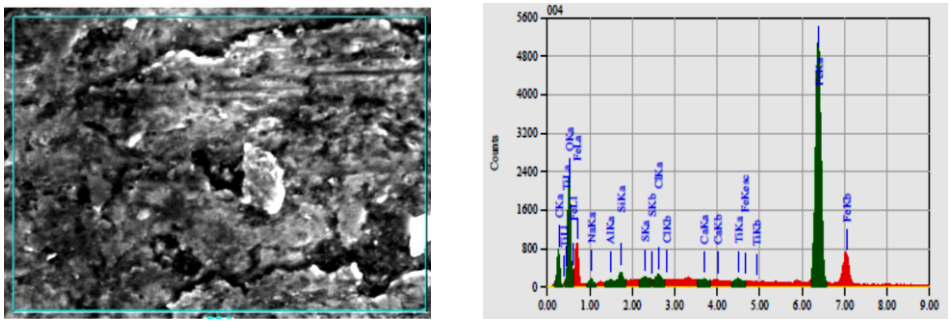

Figure 21. Photographs and graphs of fracture surfaces at location four

From the square area in Figure 21, the carbon equivalent of 12.69%, the ferrous content is 65.84%, and the presence of oxygen is 18.89%, which causes cracks and weld porosity. Compared to the standard AISI 1045 carbon equivalent material value, it is 0.65% with a ferrous content of 98.981%. The result of the analysis has shown and proved that there is an increase in the carbon equivalent value of 15.66%, an average value of oxygen element of 19.31%, and a drop in the value of the average ferrous content of 48.74%. This is the cause of the decreased reliability of the AISI 1045 shaft and triggers the occurrence of cracks and faster static brittle fracture; due to the reconditioning process with SMAW not meeting the Welding Procedure Standard.

4. CONCLUSIONS

Based on laboratory tests, it was determined that the occurrence of static brittle fracture at the corners of the AISI 1045 shaft between the 65 mm and 90 mm diameters was caused by a large number of weld defects in the form of inclusions, porosity, cold cracks in the HAZ, the presence of oxygen, and the difference in hardness between the weld metal, HAZ, and base metal, and had been for a long time. The macro-micro structure is bainite and ferrite-pearlite at the initial area of crack and fracture, while the base material is ferrite-pearlite. However, shock cold treatment promotes the formation of a martensitic structure that is strong and brittle as a trigger for static brittle fracture, and there is a difference in tensile strength between the shaft material and the electrodes utilized. Similarly, the difference in hardness level, where the hardness value of the weld material ranges from 200HV to 210 HV, in HAZ 280HV to 386 HV, and in the base material 202HV to 210HV. Reconditioning also causes a decline in the mechanical characteristics of the shaft, resulting in decreased reliability and fracture in 2,920 working hours due to a 15.66% increase in the carbon equivalent value, which should only be 0.65%. Reconditioning does not fulfill the American Welding Society's Welding Procedure Standard.

ACKNOWLEDGMENT

The authors thank the Research Center of Mining Technology, National Research and Innovation Agency of Indonesia, Jalan Ir. Sutami Km. 15 South Lampung, Lampung, Indonesia, 35361, Pekanbaru High School of Technology, Riau Science Techno Park, Regional Development Planning Agency, Research and Development of Riau Province-Indonesia, which assisted the facilities during the research, and the students who were involved in this research.

REFERENCES

[1] Messler, R. W. (2004). Welding as a Joining Process. Joining of Materials and Structures, 285 - 348. https://doi.org/10.1016/B978-075067757-8/50006-3.

[2] Kumar, S., & Singh, R. (2020). Investigation of tensile properties of shielded metal arc weldments of AISI 1018 mild steel with preheating process. Materials Today: Proceedings.Vol. 26, Part 2, Pages 209 - 222.https://doi.org/10.1016/j.matpr.2019.10.167.

[3] Sayed, A. R., Kumar, D., Shahare, G. M., Nawkhare, N. N., Bhanarkar, R. Y., Dhande, D. R., Bharadkar, U. M. (2021). Mechanical and microstructural testing of C-45 material welded by Using SMAW and GMAW Process. Materials Today: Proceedings.Vol. 38, Part 1, Pages 223-228. https://doi.org/10.1016/j.matpr.2020.07.036.

[4] Pushp Kumar Baghel. (2022). Effect of SMAW process parameters on similar and dissimilar metal welds: An overview. Heliyon. Vol. 8, Issue 12, December 2022, e12161. https://doi.org/10.1016/j.heliyon.2022.e12161.

[5] Suheni (2021). Effect of Welding Groove and Electrode Variation to the Tensile Strength and Macrostructure on 304 Stainless Steel and AISI 1045 Dissimilar Welding Joint Using SMAW Process, IOPscience. ICATECH 2021 Journal of Physics: Conference Series 2117 IOP Publishing.https://iopscience.iop.org/article/10.1088/1742-6596/2117/1/012018/pdf.

[6] N. Saini, R. Raghav, V. Bist, R.S. Mulik, M.M Mahapatra (2021). Microstructural features and mechanical properties of similar and dissimilar ferritic welded joints for ultra-supercritical power plants. International Journal of Pressure Vesselsand Piping. Vol. 194, Part B, 15 December 2021, 104556. https://doi.org/10.1016/j.ijpvp.2021.104556.

[7] Jawad, M., Jahanzaib, M., Ali, M. A., Farooq, M. U., Mufti, N. A., Pruncu, C. I. Wasim, A. (2021). Revealing The Microstructure And Mechanical Attributes of Preheated Conditions for Gas Tungsten Arc Welded AISI 1045 Steel Joints. International Journal of Pressure Vessels and Piping, 192, 104440. https://doi.org/10.1016/j.ijpvp.2021.104440.

[8] Luiz Lagares, M., Catão Silva, G., & Caldeira, L. (2020). Fusion zone microstructure image dataset of the Flux-Cored and Shielded Metal Arc Welding processes. Data in Brief, 106353.Data in Brief. Vol. 33, December 2020, 106353. https://doi.org/10.1016/j.dib.2020.106353.

[9] Kumar Singh, D., Sahoo, G., Basu, R., Sharma, V., & Mohtadi-Bonab, M. A. (2018). Investigation on the microstructure—mechanical property correlation in dissimilar steel welds of stainless steel SS 304 and medium carbon steel EN 8. Journal of Manufacturing Processes, 36, 281-292. Journal of Manufacturing Processes. Vol. 36, December 2018, Pages 281-292. https://doi.org/10.1016/j.jmapro.2018.10.018.

[10] Jorge, L. de J., Cândido, V. S., Silva, A. C. R. da, Garcia Filho, F. da C., Pereira, A. C., Luz, F. S. da, & Monteiro, S. N. (2018). Mechanical properties and microstructure of SMAW welded and thermically treated HSLA-80 steel. Journal of Materials Research and Technology. Journal of Materials Research and Technology.Vol. 7, Issue 4, October-December 2018, Pages 598-605.https://doi.org/10.1016/j.jmrt.2018.08.007.

[11] American Welding Society, Welding Handbook. Vol. 2, Welding Processes, Miami, 1995.

[12] ASM Handbook. Vol. 6, Welding, Brazing and Soldering, 1992.

[13] American Welding Society Handbook. Vol. 3, Materials and Applications Part 1, Miami, 1996.

[14] American Welding Society Handbook, volume 1, Welding Technology, Miami, 199.

[15] ASM Handbook. Vol. 1, Properties and Selection: Irons, Steels, and High-Performance Alloys, 1992.

[16] Su Y, Li W, Wang X, Ma T, Ma L, & DouX. (2019). The Sensitivity Analysis of Microstructure and Mechanical Properties to Welding Parameters for Linear Friction Welded Rail Steel Joints. Materials Science and Engineering: A, 138251. https://doi.org/10.1016/j.msea.2019.138251.

[17] Jawad M, Jahanzaib M, Ali M. A, Farooq M, Mufti N. A, Pruncu C. I, Wasim A. (2021). Revealing the Microstructure and Mechanical Attributes of Preheated Conditions for Gas Tungsten Arc Welded AISI 1045 Steel

Joints. International Journal of Pressure Vessels and Piping. Vol. 192, 104440, https://doi.org/10.1016/j.ijpvp.2021.104440.

[18] Han L, Han T, Chen G, Wang B, Sun J, & Wang Y. (2021). Influence of Heat Input on Microstructure, Hardness and Pitting Corrosion af Weld Metal in Duplex Stainless Steel Welded By Keyhole-TIG. Materials Characterization.Vol. 175, 111052. https://doi.org/10.1016/j.matchar.2021.111052.

[19] Du-Rim Eo., Jongcheon Yoon, and Hyub Lee, (2023). Heterostructure Effect at The Interface of Maraging Steel Deposited Upon Carbon Steel Via Directed Energy Deposition. Materials & Design, Vol. 225-111574. https://doi.org/10.1016/j.matdes.2022.111574.

[20] ASM Handbook, Vol. 9, Metallography and Microstructures, 1992.

[21] Robert W. Messler Jr. (2004). Chapter 6 - Welding as a Joining Process. Joining of Materials and Structures from Pragmatic Process to Enabling Technology 2004, Pages 285-348. https://doi.org/10.1016/B978-075067757-8/50006-3.

[22] Olexandr Ivanov, Pavlo Prysyazhnyuk, Liubomyr Shlapak, Sergiy Marynenko, Lyudmyla and Halyna Kramar. (2022). Researching of the Structure and Properties of FCAW Hardfacing Based on Fe-Ti-Mo-B-C Welded Under Low Current. Procedia Structural IntegrityVol. 36, Pp223-230. https://doi.org/10.1016/j.prostr.2022.01.028.

[23] Gawhar Ibraheem Khidhir, Sherko A. Baban. (2019). Efficiency of Dissimilar Friction Welded
1045 Medium Carbon Steel and 316L Austenitic Stainless Steel Joints.https://doi.org/10.1016/j.jmrt.2019.01.010.

[24] Sayed, A. R., Kumar, D. Shahare, G. M, Nawkhare N. N, Bhanarkar R. Y, Dhande D. R, Bharadkar U. M. (2020). Mechanical and Microstructural Testing of C-45 Material Welded by Using SMAW and GMAW Process. Material Toady: Proceedings. Vol. 38, Part 1, 2021, Pp. 223-228. https://doi.org/10.1016/j.matpr.2020.07.036.

[25] Muhammad Atif Makhdoom, Furqan Ahmed, Iftikhar Ahmed Channa, Aqil Inam, Fahad Riaz,
Sajid Hussain Siyal, Muhammad Ali Shar, and Abdulaziz Alhazaa. (2022). Effect of Multiple Thermal Cycles on the Microstructure and Mechanical Properties of AISI 1045 Weldments.
American Chemical Society, 7, 42313−42319.http://pubs.acs.org/journal/acsodf.

[26] Mohammad Saadati, Amir Keyvan Edalat Nobarzad, and Mohammad Jahazi. (2019). On the Hot Cracking of HSLA Steel Welds: Role of Epitaxial Growth and HAZ Grain Size. Journal of Manufacturing Processes. Vol. 41, 242–251. https://doi.org/10.1016/j.jmapro.2019.03.032.

[27] Merbin John, Ashok Kumar P, Udaya Bhat K, and Devadas Bhat P. (2021). A Study on HAZ Behaviour in 800 MPa Cold Rolled and Hot Rolled Steel Weld. Materials Today: Proceedings 44, 2985–2992.https://doi.org/10.1016/j.matpr.2021.02.124.

[28] Philip Jordan, and Chris Maharaj. (2020). Asset Management Strategy for HAZ Cracking Caused by Sigmaphase and Creep Embrittlement in 304H Stainless Steel Piping. Engineering Failure Analysis. Engineering Failure Analysis. Vol. 110, 04452.https://doi.org/10.1016/j.engfailanal.2020.104452.

[29] Ravindra Kumar, and V.K. Tewari, Satya Prakash. (). Oxidation Behavior of Base Metal, Weld Metal and HAZ Regions of SMAW Weldment in ASTM SA210 GrA1 Steel. Journal of Alloys and Compounds, Vol. 479, 432–435. https://doi.org/10.1016/j.jallcom.2008.12.110.

[30] Seung Hwan Lee, Ki Hyuk Kim, Donghyun Van, and Sangwoo Nam. (2020). Effect of C-Mn Ratio on the Maximum Hardness and Toughness in TMCP Steels with an Identical Carbon Equivalent. Journal of Materials

research and technology.Vol. 9-4:8916-8928. https://doi.org/10.1016/j.jmrt.2020.06.010.

[31] Murshid Imam, Rintaro Ueji, and Hidetoshi Fujii. (2015). Microstructural Control and Mechanical Properties in Friction Welding of Medium Carbon Low Alloy S45C Steel. Materials Science & Engineering A 636 (2015) 24–34. http://dx.doi.org/10.1016/j.msea.2015.03.089.